



ELSEVIER

Contents lists available at ScienceDirect

Optics Communications

journal homepage: www.elsevier.com/locate/optcom

Photonic crystal structures for light trapping in thin-film Si solar cells: Modeling, process and optimizations



Xing Sheng*, Lirong Z. Broderick, Lionel C. Kimerling

Department of Materials Science and Engineering, Massachusetts Institute of Technology, Cambridge, MA 02139, USA

ARTICLE INFO

Article history:

Received 25 February 2013

Received in revised form

22 July 2013

Accepted 28 July 2013

Available online 21 August 2013

Keywords:

Thin-film silicon

Solar cells

Light trapping

Photonic crystals

Self-assembly

Optimization

ABSTRACT

In this paper, we present our efforts on studying light trapping in thin-film silicon solar cells using photonic crystal (PC) based structures. Specifically, we propose a photonic backside texture combining periodic gratings and a distributed Bragg reflector (DBR). The mechanisms of this integrated photonic design are theoretically studied and compared with conventional PCs. We experimentally fabricate the texture using lithographic and self-assembled method on thin-film single crystalline Si (c-Si) and microcrystalline Si (μ c-Si) cells. We analyze the effects of the photonic textures on different cells and demonstrate the performance improvements. A numerical method is developed to explore the optimal multiscale textured surface and investigate light trapping limits in the wave optics regime. Using a detailed balance analysis, we show that it is possible to reach over 20% efficiency for 1.5 μ m Si cells through optimal device design and fabrication.

© 2013 Elsevier B.V. All rights reserved.

1. Introduction

Photovoltaic (PV) technology is considered to be a promising technique for solar energy utilization and has already achieved wide applications for space and terrestrial power generation [1]. Among all the semiconductor solar cells, silicon (Si) based solar cells have dominated most of the PV market due to the abundance and mature technology of Si. Further cost reduction requires less material usage and a thin-film Si based platform [2,3]. The efficiency of thin-film Si solar cells critically depends on optical absorption in the Si layer since single-crystalline (c-Si), amorphous (a-Si), and microcrystalline silicon (μ c-Si) have low absorption coefficients in the red and near-infrared wavelength ranges. Nowadays, thin-film Si solar cells still show inferior performances compared to their bulk c-Si based counterpart. Therefore, an effective light trapping design is indispensable to achieve high efficiency modules. Traditional light trapping schemes such as textured transparent conductive oxides (TCOs) and metal reflectors [4] lack the ability to precisely control and optimize the textured surface in experiments and numerical models. Recently, one-, two- and three-dimensional photonic crystals (1D, 2D and 3D PCs) have also been proposed to enhance the light trapping [5–

8]. Such PC structures can be optimized numerically but still remain challenging for low-cost fabrication, especially for 2D and 3D PCs. In addition, some fundamental questions have not yet been solved for light trapping and efficiency limits in thin-film Si solar cells.

This report aims to address the above questions by summarizing our recent progress on designing and fabricating light trapping structures in thin-film Si cells. We begin by introducing a light trapping design combining periodic gratings and DBR. We then review the experimentally realized devices and systematically discuss the device performances. Finally, we develop numerical models to explore the optimized photonic texture and examine the fundamental limits for light trapping and efficiency limits in thin-film Si cells.

2. Theory

Fig. 1 illustrates thin-film Si cells with different photonic crystal based back reflectors, as well as the wave propagations. Those simulation cells have periodic boundary conditions in the lateral direction, under normally incident TE polarized light (the electric field perpendicular to the incident plane) at 800 nm. The active device layer is 1.5 μ m c-Si. The electric field distributions are simulated with the finite-difference time-domain (FDTD) method [9,10]. In Fig. 1(a), 5 pairs of alternating a-Si ($n_{a-Si}=3.6$, $d_{a-Si}=56$ nm) and SiO₂ ($n_{SiO_2}=1.45$, $d_{SiO_2}=138$ nm) layers form a distributed Bragg reflector (DBR, or 1D PC). This designed DBR

* Corresponding author. Current address: Department of Materials Science and Engineering, University of Illinois at Urbana-Champaign, Urbana, IL 61801, USA. Tel.: +1 412 992 6749.

E-mail address: shengxingstars@gmail.com (X. Sheng).

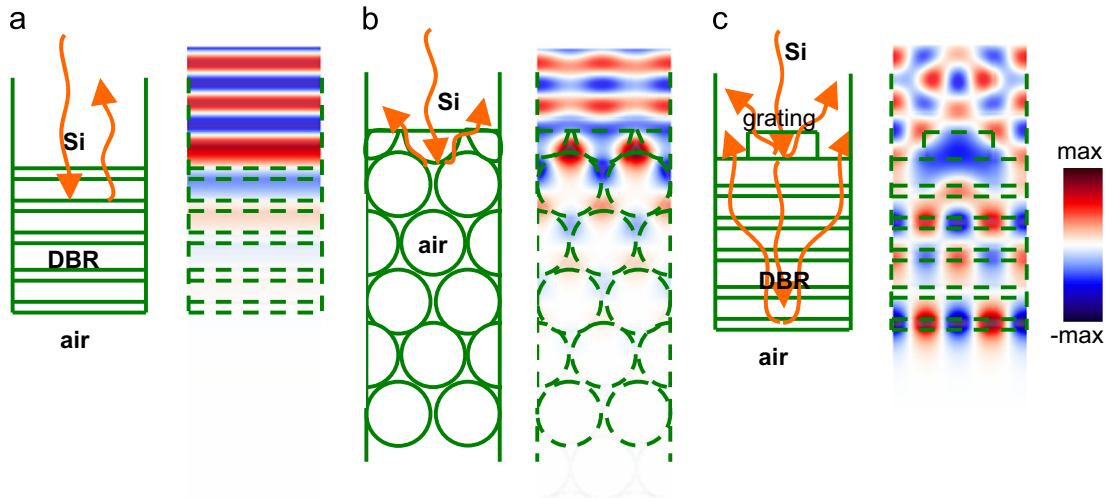


Fig. 1. Simulated electric field distribution in thin-film c-Si cells with different light trapping schemes: (a) with a DBR, made by 5 pairs of a-Si (56 nm) and SiO₂ (138 nm); (b) with a 2D PC, made by air holes embedded in Si (lattice period 350 nm, hole radius 168 nm); and (c) with grating (period 800 nm and thickness 100 nm) and DBR [12].

exhibits a complete photonic bandgap for both TE and TM polarized light approximately from 650 nm to 1000 nm [11,12]. When light is incident on such a DBR from the thin-film c-Si, it is totally reflected. The second design illustrated in Fig. 1(b) consists of a 2D photonic crystal in the back, made of a triangular lattice of cylindrical air holes embedded in Si (lattice period $a=350$ nm, hole radius $r=0.48$, $a=168$ nm). Such an optimized 2D photonic crystal structure can provide a complete bandgap for both TE and TM light [13], in the range between 673 nm and 814 nm. Furthermore, the light incident on the 2D PC ($\lambda=800$ nm) is not only totally reflected, but also diffracted because of the periodicity introduced in the lateral direction, further increasing the light path length. Therefore, 2D PC structures can provide better light trapping performance than a 1D DBR at specific wavelengths. However, thin-film Si cells need a reflecting and scattering component that can work in a broad band covering the entire red and near-infrared spectral range. Compared to the DBR, the optimized 2D PC only has a very narrow bandgap [13] and cannot provide desired light trapping for broad band applications. Furthermore, experimentally fabricating such a structure has lots of technical challenges and is not feasible for low cost and large area PV applications. In order to combine the benefits from both 1D and 2D PC structures, we propose an integrated PC structure illustrated in Fig. 1(c), including the DBR in Fig. 1(a) as well as a periodic grating [14,15]. Specifically, the grating is assumed to be made of Si and SiO₂, with a period of 800 nm, a duty cycle of 0.5 and a thickness of 100 nm. The operational principles of such an integrated PC structure are explained in Fig. 1(c). When the grating layer is embedded between the Si and DBR, scattering is introduced. The light is not only scattered backward but also forward into the DBR, due to the band folding introduced by the periodic grating [12]. However, no field can penetrate into the bottom air layer, and almost all the waves are totally reflected back at the DBR/air interface and eventually get trapped in the thin-film device. Therefore, the texture PC structure in Fig. 3(c) combines the benefits of the wide reflection gap of the DBR and the strong scattering of the grating, leading to effective broad band light trapping. In addition, this structure can be more easily fabricated compared to the complicated 2D PCs, with a potential for low-cost productions. The DBR structure also shows superior performance compared to conventional metal reflectors, because of the high reflectivity (nearly 100% for DBR vs. about 80–90% for metals) in the desired spectral range [12].

3. Experiment

3.1. Thin-film c-Si cells with lithographically defined gratings

Our proposed grating and DBR structures integrated with 5 μm thick c-Si solar cells [16] are shown in Fig. 2(a). To fabricate such a device, silicon-on-insulator (SOI) wafers are used as the starting materials. Processing of the SOI active layer includes grating formation with interference lithography, followed by reactive ion etching, DBR deposition using plasma enhanced chemical vapor deposition (PECVD), bonding the active layer to a new handle wafer, removal of the original handle wafer, forming an antireflective coating (ARC) on the newly exposed Si surface, lateral p-i-n junction creation by ion implantation, and metallization with interdigitated contacts for both p-doped and n-doped regions on the top surface. The cross-sectional TEM image of the fabricated PC structure is shown in Fig. 2(b). The structural parameters of the PC structures are determined by numerical simulations and optimizations [6,15]. The cells without any reflectors and only with a DBR are also fabricated for comparison.

Current–voltage (J – V) measurements in Fig. 2(c) demonstrate that each back structure improves absorption and cell efficiency, with the cell combining grating and DBR achieved the highest short-circuit current J_{sc} of 17.5 mA/cm², compared to 14.7 mA/cm² for the reference cell. The measured power conversion efficiency is increased from 7.68% for the reference cell to 8.82% for the cell with grating and DBR. A relative efficiency enhancement of 14.8% is obtained. The measured EQE spectra shown in Fig. 2(d) also reveal that the combined grating and DBR structure obtains the highest absorption enhancement in the spectral range from 600 nm to 1000 nm.

3.2. Thin-film micro-crystalline Si cells with self-assembled gratings

The thin-film c-Si solar cells made from SOI wafers demonstrate relatively high efficiencies; however, the process and starting materials are not economically viable for scale-up production. In addition, the periodic grating in Fig. 2(b) is lithographically defined, which further increases the production cost. In Fig. 3 we apply our design on low-cost $\mu\text{c-Si}$ solar cells, introducing a self-assembled process to fabricate the similar light trapping structures [11]. The $\mu\text{c-Si}$ solar cell structure is shown in Fig. 3(a). The active device layer is a 1.5 μm thick $\mu\text{c-Si}$ p-i-n junction, produced by a

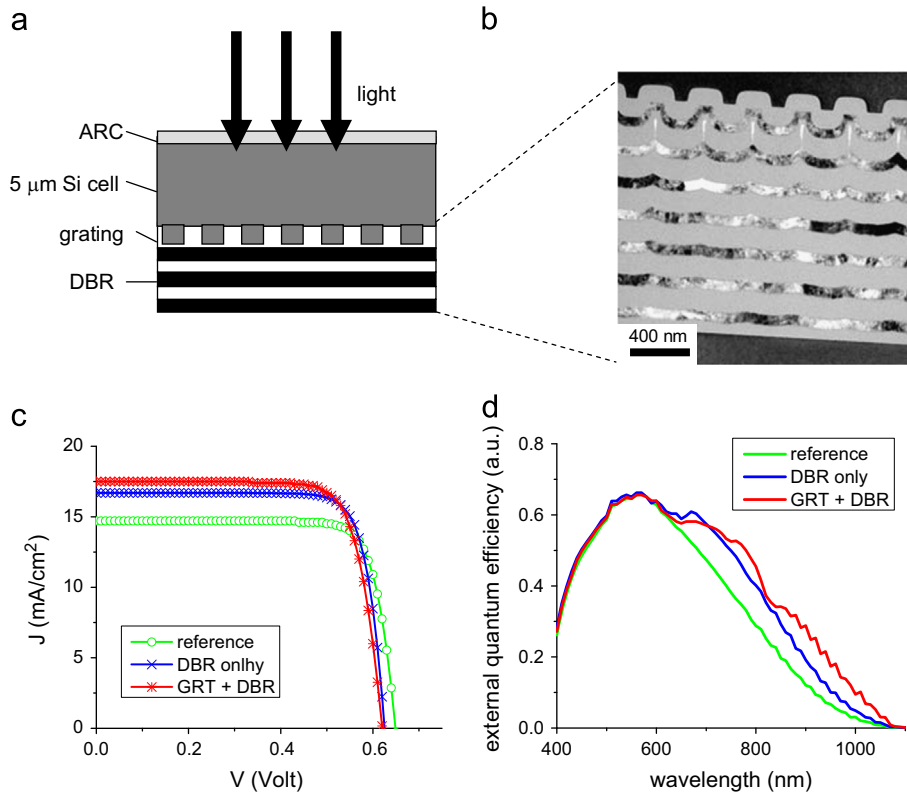


Fig. 2. (a) Schematic of the fabricated thin-film c-Si cell combining grating and DBR; (b) cross-sectional TEM image of the grating defined by lithographic patterning and the DBR made of multilayered SiO₂ and Si; performances of c-Si cells with various back structures: the reference cell without grating (GRT) and DBR, the cell with only DBR, and the cell with both GRT and DBR; (c) *J*-*V* curves measured under AM1.5G illumination; and (d) EQE spectra using monochromatic light [16].

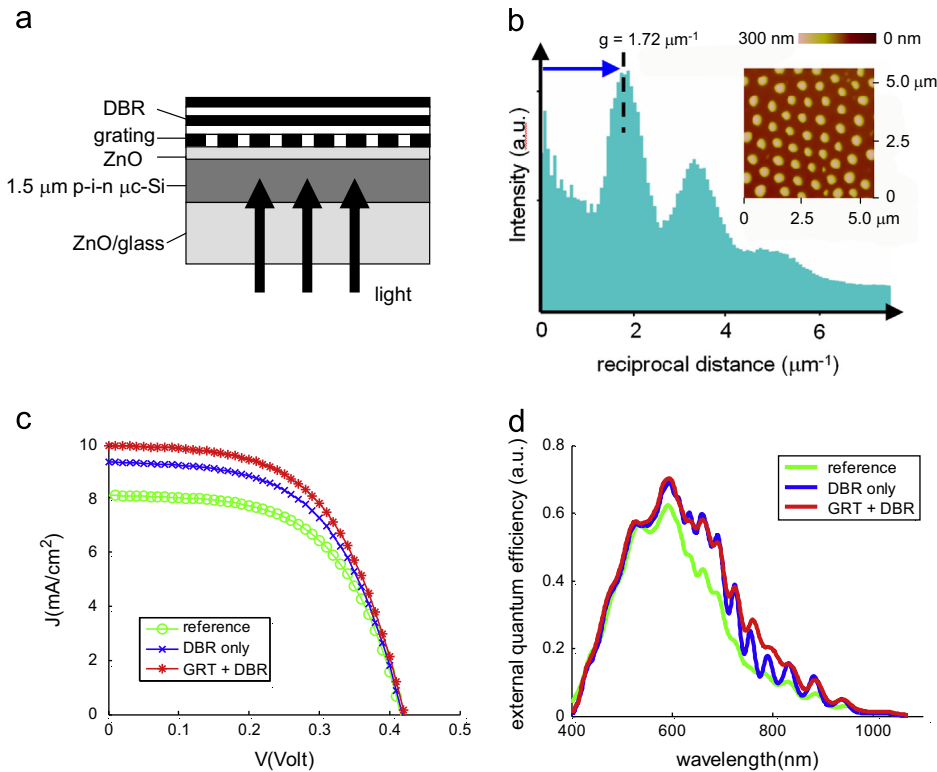


Fig. 3. (a) Schematic of the thin-film μc-Si cell with self-assembled grating and DBR; (b) AFM image of the fabricated a-Si grating pattern and FFT intensity profile of the AFM image; performances of μc-Si cells with various back structures: the reference cell without GRT and DBR, the cell with only DBR, and the cell with both GRT and DBR; (c) *J*-*V* curves measured under AM1.5G illumination; and (d) EQE spectra using monochromatic light [11].

commercial PECVD system. Two ZnO:Al based transparent conductive oxide layers work as top and bottom contacts. The grating and DBR in the backside are firstly optimized by numerical simulations, in which we find the optimal grating period is about 700 nm. To non-lithographically fabricate the submicron grating layer, we use a self-assembled technique based on anodic aluminum oxide (AAO) [17]. The AAO has a porous structure with a hexagonal pattern, of which the period can be determined by the electrochemical process [18]. Through the fabricated AAO mask, we evaporate a-Si to form the grating. The AFM image shown in the inset of Fig. 3(b) represents the deposited a-Si pattern. Based on the 2D Fast Fourier Transformation (FFT) spectrum in Fig. 3(b), we can calculate the grating period to be $\Lambda = 2/\sqrt{3}g = 670$ nm, similar to our numerically optimized result. Subsequently, 5 pairs of alternating SiO₂ (130 nm) and a-Si (40 nm) layers are deposited as a DBR.

The performances of μ c-Si solar cells with different back structures are shown in Fig. 3(c) and (d). The J - V curves in Fig. 3(c) show the cell with self-assembled grating and DBR has the highest J_{sc} and the highest efficiency among all the devices. Compared to the reference cell without any backside reflectors, the planar DBR can achieve an efficiency relative increase of 13%, while the cell with optimal grating and DBR shows the highest performance with a relative improvement of 21%. The external quantum efficiency (EQE) spectra plotted in Fig. 3(d) further confirm with the J - V measurements. All of the cells exhibit similar EQE values at short wavelengths (below 500 nm), while significant EQE enhancements can be observed from 600 nm to 900 nm for the cells with designed PC reflectors. Strong Fabry-Perot interference peaks appear for the device with a planar DBR. When the grating layer is added, light diffraction occurs and light path length is further increased, obtaining an even higher efficiency.

3.3. Discussion

In Table 1, we summarize and compare the performances for c-Si and μ c-Si cells we described in Sections 3.1 and 3.2, respectively. The J - V relationship for a cell under solar illumination can be simplified as

$$J = J_{ph} - J_0 \left[\exp\left(\frac{eV}{kT}\right) - 1 \right] \quad (1)$$

In Eq. (1), J_{ph} is the photogenerated current, which is directly related to the absorption of the active solar cell devices. The short-circuit current J_{sc} is defined as

$$J_{sc} = J(V = 0) = J_{ph} \quad (2)$$

Therefore, J_{sc} is determined by the light trapping performance of the photonic structures. In Sections 3.1 and 3.2, μ c-Si cells have relatively low J_{sc} compared to c-Si cells, mainly because of the thinner active device layer (1.5 μ m vs. 5 μ m), recombinations at defect centers (grain boundaries), and the parasitic absorption in the conductive oxide layers. For both c-Si and μ c-Si cells, introducing DBR and grating structures increases J_{sc} .

Table 1
Summary of measured characteristics for 5 μ m c-Si cells and 1.5 μ m μ c-Si cells with different backside structures.

Cell type		J_{sc} (mA/cm ²)	V_{oc} (V)	Efficiency (%)
5 μ m c-Si	Reference	14.7	0.649	7.68
	DBR only	16.7 \uparrow	0.625 \downarrow	8.39 \uparrow
	GRT+DBR	17.5 \uparrow	0.621 \downarrow	8.82 \uparrow
1.5 μ m μ c-Si	Reference	8.09	0.416	1.93
	DBR only	9.32 \uparrow	0.418 \uparrow	2.18 \uparrow
	GRT+DBR	9.94 \uparrow	0.422 \uparrow	2.34 \uparrow

On the other hand, when $J = 0$, we can get open-circuit voltage V_{oc}

$$V_{oc} = \frac{kT}{e} \ln\left(\frac{J_{ph}}{J_0} + 1\right) \quad (3)$$

Therefore, V_{oc} is not only dependent on the photocurrent J_{ph} , but also dependent on the reverse bias saturation current J_0 . Device fabrication and materials qualities determine the number of recombination centers in the device, therefore strongly influence J_0 . Due to the difference in crystallinity, μ c-Si based cells show lower V_{oc} than c-Si cells (about 0.4 V vs. 0.6 V). Furthermore, photonic textures have different effects on these two types of Si cells. For c-Si cells, grating fabrication and DBR deposition involve active device etching, which results in more surface defects, higher surface recombination rate and larger J_0 . Compared to the reference flat cell, cells with grating and/or DBR structures have lower V_{oc} . However, in the 1.5 μ m μ c-Si cells, V_{oc} is not affected by the backside structures. This is because the self-assembled gratings and DBR are only deposited on the ZnO:Al conductive layer, without affecting the active μ c-Si layer. Therefore, the enhanced light trapping (J_{ph}) in μ c-Si cells is not accompanied by increased surface recombination, unlike the textured Si interfaces in c-Si cells.

4. Structure optimization

In previous sections, we have designed and experimentally demonstrated the effectiveness of using periodic gratings (lithographically defined and self-assembled) and DBR for light trapping in thin-film Si. Recently, various kinds of periodic textures have been proposed in literatures, including wires, spheres, cones, etc. [18–22]. Among different textures, probably simple shapes like triangular or rectangular gratings do not have the highest performances. Furthermore, what is the ultimate limit for the absorption in the thin-film silicon, and what is the optimal design that can reach this limit? These are still debatable topics which attract both academic and industrial interests [23–26]. To further optimize the light trapping performance of a periodic structure, we investigate an arbitrarily shaped texture [27]. In principle, any arbitrarily shaped multiscale 1D periodic texture, described by the function $H(x)$, can be expanded in terms of its Fourier series

$$H(x) = \sum_{n=1}^{\infty} \left[A_n \sin\left(\frac{2\pi n}{\Lambda}x\right) + B_n \cos\left(\frac{2\pi n}{\Lambda}x\right) \right] \quad (4)$$

where Λ is the period of the simulation cell, and $A_1, B_1, A_2, B_2, \dots$ are the coefficients for different order Fourier components. Under the weak-absorption limit, the performance of the texture can be characterized by the dimensionless enhancement factor F , which is the averaged absorption in a certain spectral range (λ_1, λ_2) divided by the single-pass absorption αd in a thin film with a thickness d

$$F = \frac{1}{\lambda_2 - \lambda_1} \frac{\int_{\lambda_1}^{\lambda_2} A(\lambda) d\lambda}{\alpha d} \quad (5)$$

Because the absorption spectrum $A(\lambda)$ can be numerically calculated for any given device texture $H(x)$, F is directly related to these structural parameters

$$F = F(A_1, B_1, A_2, B_2, \dots, \Lambda) \quad (6)$$

Therefore, we can optimize the device performance F by tuning the parameters ($A_1, B_1, A_2, B_2, \dots$ and Λ). Practically, we only choose the first 5 orders, i.e., from (A_1, B_1) to (A_5, B_5), and set higher-order Fourier coefficients to zero. An example of the optimization process is shown in Fig. 4(a). Here we start with a planar 2D device structure with a period Λ , consisting of air (semi-infinite), 1.5 μ m c-Si, 0.5 μ m SiO₂ and a perfect reflector on the backside. The c-Si layer is assumed to be weakly absorptive, with a constant absorption coefficient. The unit cell is illuminated under normal

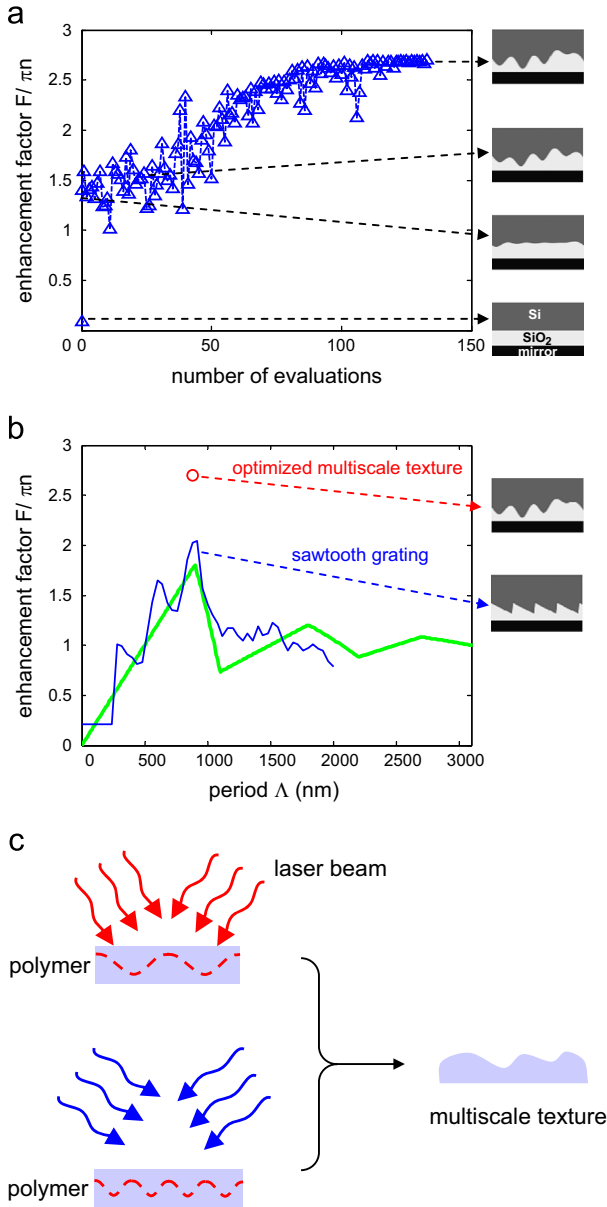


Fig. 4. (a) Convergence trends for enhancement factor F optimization starting with a flat structure; (b) comparison of obtained F for our optimized texture with results for sawtooth gratings and theories based on Yu's model [27]; and (c) our proposed method using multi-step interference lithography to fabricate the optimized texture.

incidence by TE polarized light from 900 nm to 1100 nm. We simulate the structure using the FDTD method combined with a nonlinear optimization toolbox NLOpt [10,28]. In the simulation, we keep the average thickness of the c-Si as a constant (1.5 μm), while varying the other structural parameters (SiO_2 thickness, period Λ and the first 5-order Fourier coefficients), base on an algorithm called constrained optimization by linear approximation (COBYLA) [29]. Fig. 4(a) also illustrates the shapes of the multiscale textures after different number of iterations. In this particular optimization, F converges after about 100 iterations, and the best found F is $2.7\pi n$. It should be noted that this obtained optimal $F=2.7\pi n$ is a local optimum, and it is infeasible to guarantee that the global optimum has been obtained, so the obtained result only represent a lower bound on the attainable performance.

Fig. 4(b) compares our optimized result based on multiscale textures with the best simulation results performed on a simple

sawtooth grating with different period Λ . Predictions for asymmetric gratings based on a generalized model developed by Yu et al. [30] are also shown, derived from

$$F(\Lambda) = \frac{1}{\lambda_2 - \lambda_1} \int_{\lambda_1}^{\lambda_2} \left(\frac{\frac{\Lambda}{\lambda}}{|\frac{\Lambda}{\lambda}| + \frac{1}{2}} \right) d\lambda \pi n \quad (7)$$

As illustrated, the results for sawtooth gratings follow a trend similar to Yu's analytical results, peaking at around $\Lambda=900$ nm, while F for gratings with optimized multiscale texture ($2.7\pi n$) exceeds the optimal sawtooth gratings as well as the analytical results. This is because our optimized periodic texture violates isotropic coupling assumption in the analytical model [30], thus obtaining higher performance at normal incidence while sacrificing the performance at larger incident angles [27].

To fabricate the optimized multiscale texture surface obtained in the above numerical simulations, facile and large-area techniques should be introduced. A rapid growing technique is nanoimprint [31], which can create arbitrary patterns on soft materials using prefabricated hard molds. The hard molds can be reused for multiple printing processes, greatly reducing the cost. Alternatively, we propose another fabrication method illustrated in Fig. 4(c) by modifying interference lithography [32]. It is a well-known technique of using coherent laser beams to form periodic patterns on photosensitive polymers. The feature sizes (period, phase, depth, etc.) are dependent on the optical configurations (laser wavelength, incident angle, exposure time, etc.). Therefore, different patterns, which correspond to different Fourier components in our numerical model, can be superimposed on the same polymer layer by applying multiple exposures. By tuning the laser beam parameters, the developed polymer pattern will render a similar shape of texture matching our optimized structure.

5. Fundamental limits

This article is mainly focused on the light trapping issues, that is, designing a solar cell structure that can absorb as much light as possible and generate larger J_{sc} . Ultimately, we not only want to maximize the J_{sc} , but also the power conversion efficiency of the solar cell. Theoretical analysis for efficiency limits in Si cells has been discussed extensively in literature (for example, see Ref. [49]). Here we propose a more generic prediction about the fundamental efficiency limits of a single junction solar cell. We extend Eq. (1) based on the generalized Shockley–Queisser theory [33–35], and write the current generated by a solar cell as a balance between photon absorption and carrier recombination

$$J = J_{\text{photon}} - J_{\text{recombination}} = e \int_0^{\lambda_g} s(\lambda) A(\lambda) d\lambda - \frac{1}{\eta_{\text{ext}}} \frac{2\pi e E_g^2 kT}{h^3 c^2} \exp\left(\frac{-E_g}{kT}\right) \left[\exp\left(\frac{eV}{kT}\right) - 1 \right] \quad (8)$$

where e is the unit charge for an electron, λ_g is the cutoff wavelength for absorption (corresponding to the material bandgap E_g), $s(\lambda)$ is the standard AM1.5G solar spectrum [36], $A(\lambda)$ is the absorption spectrum of the solar cell (depending on the material absorption coefficient and device light trapping design), h is the Planck's constant, c is speed of light in vacuum, E_g is the bandgap of the semiconductor, k is the Boltzmann constant and T is the environment temperature. η_{ext} is the external radiation efficiency, which is the ratio of radiative recombination to the total recombination (including radiative and non-radiative) [35]. It depends on the properties of semiconductors (internal radiation efficiency, Auger recombination, free carrier absorption, etc.) and device structure design. Direct bandgap semiconductors like GaAs can have very high η_{ext} [37,48], while indirect bandgap semiconductors like Si and Ge typically have low η_{ext} (around 1% even for the best devices) [38,48]. At room

temperature ($T=300$ K), Eq. (8) represents the ideal J - V relationship for a single junction semiconductor solar cell. Therefore, the ideal efficiency of the solar cell is the maximum output power divided by the incident solar energy

$$\eta = \frac{J_{max} V_{max}}{\int_0^{\infty} s(\lambda) d\lambda} \quad (9)$$

As an ideal case, we assume an infinitely thick device that can absorb all the photons with energy above the bandgap, then $A(\lambda)=100\%$. Fig. 5(a) plots the detailed balance efficiency limit η as a function of E_g for $\eta_{ext}=100\%$ and $\eta_{ext}=1\%$, respectively. Under AM1.5G spectrum, the maximum efficiency for a single junction solar cell with $\eta_{ext}=100\%$ is 33.8% with a bandgap of 1.34 eV, while today's best GaAs cell ($E_g=1.43$ eV) has an efficiency of 28.8% [39]. For semiconductors with higher non-radiative recombination rates, the low η_{ext} significantly reduces the efficiency limits. Especially for low bandgap semiconductors ($E_g < 1.5$ eV), there is an efficiency drop of about 5% when η_{ext} decreases from 100% to 1%. With the assumption of $\eta_{ext}=1\%$, we can get the maximum efficiency for Si is 28.9%, while the best experimental cell has an efficiency of 25.0% [40].

When real thin-film solar cells are considered, the light absorption $A(\lambda)$ in Eq. (8) will also be a limiting factor for cell efficiency. For thin-film Si, this issue is severe because of its nature of indirect bandgap. As we discussed previously, absorption in the weak absorption range is determined by the fundamental light trapping limits. If isotropic incident light is considered, Lambertian limits are applicable and approximately [41]

$$A(\lambda) = \frac{1 - \exp[-4\alpha(\lambda)d]}{1 - \left(1 - \frac{1}{n^2}\right) \exp[-4\alpha(\lambda)d]} \quad (10)$$

where $\alpha(\lambda)$ is the absorption coefficient of c-Si [42]. Based on Eqs. (8), (9) and (10), we can calculate the efficiency limits for Si cells as a function of film thickness, as shown in Fig. 5(b). The maximum efficiency critically depends on the thickness of the absorbing layer, specifically for Si without any light trapping schemes (single pass condition). However, light trapping design (Lambertian texture, for example) can greatly overcome the absorption issue for Si and improve the efficiency. Indicated in Fig. 5(a), the maximum efficiency for a 1.5 μm thin-film c-Si cell is estimated to be 21.8%, which is much higher than the practical efficiencies obtained by experimental cells of ours and others [3,31]. In addition, the classical light trapping limits can be exceeded in restricted spectral and angular ranges, as we demonstrated for a 2D model in Section 4. Therefore, efficiency can be further improved for thin-film Si cells with advanced light

trapping design, and more than 20% can be obtained for 1.5 μm thin-film Si cells.

6. Conclusions

In this paper, we highlight our recent research progress in designing, fabricating and optimizing photonic textures for light trapping in thin-film Si solar cells. We propose a photonic crystal based texture combining a grating and a DBR in the backside of thin-film Si device for effective light absorption enhancement. The light trapping mechanism of this photonic structure is understood by electromagnetic wave theories and compared with conventional 1D and 2D photonic crystals. The designed structures are implemented on thin-film c-Si and $\mu\text{c-Si}$ based solar cells using lithographic and low-cost self-assembled methods, respectively. Solar cell performance measurements demonstrate the absorption and efficiency improvements introduced by the combined grating and DBR, and the effects of surface textures on V_{oc} are also explored.

We also explore the fundamental performance limits for thin-film Si solar cells. We develop a deterministic method to optimize arbitrary irregular periodic textures with combined multiple periods by multi-parameter optimization. For normal incidence, our optimized multiscale texture in two dimensions (2D) exhibits a considerably larger absorption enhancement compared to a recent generalized light trapping model for periodic structures in finite spectral range. We further modify the detailed balance limit to predict the ultimate efficiency for thin-film Si solar cells. Considering non-radiative recombination and advanced light trapping, we conclude that a 1.5 μm Si cell with more than 20% efficiency is achievable under one sun illumination.

In addition to photovoltaics, the presented numerical and experimental approaches can be used for light management in various optoelectronic applications, including light emitting diodes [43], photodetection [44], and information technology [45]. In future, many efforts can be explored to increase the performance for practical thin-film Si cells. As we have discussed, materials quality is the key to reduce non-radiative recombination and increase V_{oc} , so c-Si is more advantageous than $\mu\text{c-Si}$ and a-Si. Another interesting direction is to utilize special techniques like layer transfer approaches [46,47] to fabricate thin-film c-Si cells which have the ideal device quality at an acceptable manufacture cost. To further enhance thin-film absorption, the optimization methods we establish can be adapted for real 3D device. The optimized multiscale photonic structures can be fabricated by soft imprint techniques or a novel multi-step interference lithographic method as we propose in

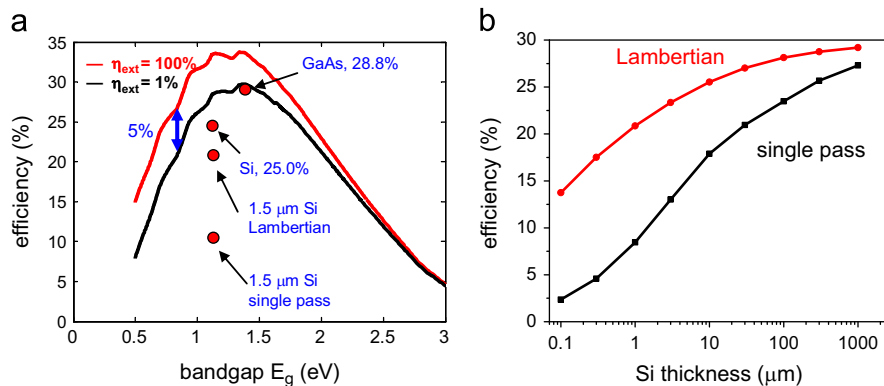


Fig. 5. (a) Detailed balance efficiency limit for semiconductors with different bandgaps under AM1.5G spectrum. The world record efficiencies to date for Si and GaAs cells as well as predicted efficiency limits for 1.5 μm c-Si cells are indicated [39]; and (b) efficiency limit for Si cells as a function of Si film thickness.

Fig. 4(c). We believe the combined calculation and fabrication methods can provide a guideline for making a thin-film Si cell that can potentially approach the theoretical efficiency limit.

Acknowledgments

We thank Massachusetts Institute of Technology Energy Initiative (MITEI), Robert Bosch LLC, and the Masdar Institute of Science and Technology for financial support.

References

- [1] A. Luque, S. Hegedus, *Handbook of Photovoltaic Science and Engineering*, Wiley, England, 2011.
- [2] R. Brendel, *Thin-Film Crystalline Silicon Solar Cells: Physics and Technology*, Wiley-VCH Verlag GmbH & Co. KGaA, Weinheim, 2003.
- [3] R. Schropp, M. Zeman, *Amorphous and Microcrystalline Silicon Solar Cells: Modeling, Materials, and Device Technology*, Kluwer Academic Publishers, Massachusetts, USA, 1998.
- [4] H. Keppner, J. Meier, P. Torres, D. Fischer, A. Shah, *Applied Physics A* 69 (1999) 169.
- [5] J. M. Gee, *Proceedings of the 29th IEEE Photovoltaic Specialists Conference (2002)* pp. 150.
- [6] P. Bermel, C. Luo, L. Zeng, L.C. Kimerling, J.D. Joannopoulos, *Optics Express* 15 (2007) 16986.
- [7] P.G. O'Brien, N.P. Kherani, A. Chutinan, G.A. Ozin, S. John, S. Zukotynski, *Advanced Materials* 20 (2008) 1577.
- [8] J. Upping, A. Bielawny, R.B. Wehrspohn, T. Beckers, R. Carius, U. Rau, S. Fahr, C. Rockstuhl, F. Lederer, M. Kroll, T. Pertsch, L. Steidl, R. Zentel, *Advanced Materials* 23 (2011) 3896.
- [9] A. Taflov, S.C. Hagness, *Computational Electrodynamics*, 2nd ed., Artech House, Norwood, MA, 2000.
- [10] A.F. Oskooi, D. Roundy, M. Ibanescu, P. Bermel, J.D. Joannopoulos, S.G. Johnson, *Computer Physics Communications* 181 (2010) 687.
- [11] X. Sheng, J. Liu, I. Kozinsky, A.M. Agarwal, J. Michel, L.C. Kimerling, *Advanced Materials* 23 (2011) 843.
- [12] X. Sheng, S.G. Johnson, L.Z. Broderick, J. Michel, L.C. Kimerling, *Applied Physics Letters* 100 (2012) 111110.
- [13] J.D. Joannopoulos, S.G. Johnson, J.N. Winn, R.D. Meade, *Photonic Crystals: Molding the Flow of Light*, 2nd ed., Princeton University Press, New Jersey, USA, 2008.
- [14] L. Zeng, Y. Yi, C. Hong, J. Liu, N. Feng, X. Duan, L.C. Kimerling, B.A. Alamariu, *Applied Physics Letters* 89 (2006) 111111.
- [15] N.N. Feng, J. Michel, L. Zeng, J. Liu, C.Y. Hong, L.C. Kimerling, X. Duan, *IEEE Transactions on Electron Devices* 54 (2007) 1926.
- [16] L. Zeng, P. Bermel, Y. Yi, B.A. Alamariu, K.A. Broderick, J. Liu, C. Hong, X. Duan, J.D. Joannopoulos, L.C. Kimerling, *Applied Physics Letters* 93 (2008) 221105.
- [17] X. Sheng, J. Liu, N. Coronel, A.M. Agarwal, J. Michel, L.C. Kimerling, *IEEE Photonics Technology Letters* 22 (2010) 1394.
- [18] H. Masuda, K. Yada, A. Osaka, *Japanese Journal of Applied Physics* 37 (1998) L1340.
- [19] L. Tsakalacos, J. Balch, J. Fronheiser, B.A. Korevaar, O. Sulima, J. Rand, *Applied Physics Letters* 91 (2007) 233117.
- [20] M.D. Kelzenberg, S.W. Boettcher, J.A. Petykiewicz, D.B. Turner-Evans, M.C. Putnam, E.L. Warren, J.M. Spurgeon, R.M. Briggs, N.S. Lewis, H. A. Atwater, *Nature Materials* 9 (2010) 239.
- [21] B.G. Prevo, E.W. Hon, O.D. Velev, *Journal of Materials Chemistry* 17 (2007) 791.
- [22] J. Zhu, C.M. Hsu, Z. Yu, S. Fan, Y. Cui, *Nano Letters* 10 (2010) 1979.
- [23] E. Yablonovitch, *Journal of the Optical Society of America* 72 (1982) 899.
- [24] H.R. Stuart, D.G. Hall, *Journal of the Optical Society of America A* 14 (1997) 3001.
- [25] Z. Yu, A. Raman, S. Fan, *Proceedings of the National Academy of Sciences* 107 (2010) 17491.
- [26] X. Sheng, J. Hu, J. Michel, L.C. Kimerling, *Optics Express* 20 (2012) A496.
- [27] X. Sheng, S.G. Johnson, J. Michel, L.C. Kimerling, *Optics Express* 19 (2011) A841.
- [28] S.G. Johnson, *The NLOpt nonlinear-optimization package*. (<http://ab-initio.mit.edu/nlopt>).
- [29] M.J.D. Powell, *Acta Numerica* 7 (1998) 287.
- [30] Z. Yu, A. Raman, S. Fan, *Optics Express* 18 (2010) A366.
- [31] C. Battaglia, J. Escarre, K. Soderstrom, M. Charriere, M. Despeisse, F. Haug, C. Ballif, *Nature Photonics* 5 (2011) 535.
- [32] S. Brueck, *Proceedings of the IEEE* 93 (2005) 1704.
- [33] W. Shockley, H. Queisser, *Journal of Applied Physics* 32 (1961) 510.
- [34] C. Henry, *Journal of Applied Physics* 51 (1980) 4494.
- [35] O.D. Miller, E. Yablonovitch, *IEEE Journal of Photovoltaics* 2 (2012) 303.
- [36] ASTM G173-03, *Standard Tables for Reference Solar Spectral Irradiances: Direct Normal and Hemispherical on 37° Tilted Surface*, ASTM International, West Conshohocken, Pennsylvania, 2005.
- [37] I. Schnitzer, E. Yablonovitch, C. Caneau, T.J. Gmitter, *Applied Physics Letters* 62 (1993) 131.
- [38] M.A. Green, J. Zhao, A. Wang, P.J. Reece, M. Gal, *Nature* 412 (2001) 805.
- [39] M.A. Green, K. Emery, Y. Hishikawa, W. Warta, E.D. Dunlop, *Progress in Photovoltaics: Research and Applications* 21 (2013) 1.
- [40] J. Zhao, A. Wang, M.A. Green, *Progress in Photovoltaics: Research and Applications* 7 (1999) 471.
- [41] M. Green, *Progress in Photovoltaics: Research and Applications* 10 (2002) 235.
- [42] E. Palik, *Handbook of Optical Constants of Solids*, Academic Press, San Diego, USA, 1998.
- [43] X. Sheng, L.Z. Broderick, J. Hu, L. Yang, A. Eshed, E.A. Fitzgerald, J. Michel, L.C. Kimerling, *Optics Express* 19 (2011) A701.
- [44] J. Wang, J. Hu, X. Sun, A. Agarwal, L.C. Kimerling, *Optics Letters* 35 (2010) 742.
- [45] R. Kirchain, L.C. Kimerling, *Nature Photonics* 1 (2007) 303.
- [46] J. Yoon, A. Baca, S. Park, P. Elvikis, J. Geddes, L. Li, R. Kim, J. Xiao, S. Wang, T. Kim, M. Motala, B. Ahn, E. Duoss, J. Lewis, R. Nuzzo, P. Ferreira, Y. Huang, A. Rockett, J.A. Rogers, *Nature Materials* 7 (2008) 907.
- [47] S.W. Bedell, D. Shahrjerdi, B. Hekmatshoar, K. Fogel, P.A. Lauro, J.A. Ott, N. Sosa, D. Sadana, *IEEE Journal of Photovoltaics* 2 (2012) 141.
- [48] M. Green, *Progress in Photovoltaics: Research and Application* 20 (2012) 472.
- [49] T. Tiedje, E. Yablonovitch, G.D. Cody, B.G. Brooks, *IEEE Transactions on Electron Devices* 31 (1984) 711.